The dynamics of open-shell Van der Waals complexes

Marie-Lise DubernetDavid FlowerJeremy M. Hutson

Citation: The Journal of Chemical Physics **94**, 7602 (1991); doi: 10.1063/1.460147
View online: http://dx.doi.org/10.1063/1.460147
View Table of Contents: http://aip.scitation.org/toc/jcp/94/12
Published by the American Institute of Physics

The dynamics of open-shell Van der Waals complexes

Marie-Lise Dubernet
Departments of Physics and Chemistry, University of Durham, South Road, Durham, DH1 3LE, England
David Flower
Department of Physics, University of Durham, South Road, Durham, DH1 3LE, England
Jeremy M. Hutson
Department of Chemistry, University of Durham, South Road, Durham, DH1 3LE, England

(Received 3 December 1990; accepted 20 February 1991)

The theory of Van der Waals complexes formed from atoms and open-shell (Σ and Π) diatomic molecules is developed, paying particular attention to the quantum numbers that are conserved in the complex and the angular momentum coupling cases that may be observed. Complexes formed from diatoms in multiplet Σ states may exhibit several different coupling schemes closely analogous to Hund's coupling cases for diatomic molecules. Complexes formed from diatoms in Π states usually exhibit a coupling scheme in which the (signed) projection P of the diatom angular momentum j onto the intermolecular axis is nearly conserved. Correlation diagrams showing the bending energy levels as a function of potential anisotropy are given for complexes containing diatomic molecules in both Σ and Π states. The transition from free internal rotor quantum numbers to near-rigid bender quantum numbers with increasing anisotropy is investigated. The cases of Ar–OH and Ne–OH are considered as examples.

I. INTRODUCTION

The spectra of Van der Waals complexes involving closed-shell molecules have provided a very rich source of information on anisotropic intermolecular forces.[1] Detailed information has been obtained for a range of systems, including the rare gas–H_2,[2–4] rare gas–hydrogen halide[5–12] and rare gas–H_2O (Refs. 13 and 14) systems. There has recently been much interest in complexes of open-shell molecules, especially Ar–OH, for which Lester and co-workers[15–19] and Fawzy and Heaven[20,21] have obtained electronic spectra correlating with the $A\,^2\Sigma \leftarrow X\,^2\Pi_{3/2}$ band system of OH. Electronic and infrared spectra of Ar–OH have been simulated by Chakravarty *et al.*[22,23] using accurate bound state calculations on *ab initio* potential surfaces calculated by Esposti and Werner.[24] Bowman *et al.*[25] have used the experimental spectra to obtain an interaction potential for Ar interacting with OH in its $A\,^2\Sigma$ state. In addition, Heaven and co-workers have obtained spectra of Ne–OH,[26] Ne–CN,[27] and Ar–CN.[28] There is also much interest in the microwave and infrared spectra of systems of this type, which would provide detailed information on the potential energy surfaces involved. Mills *et al.*[29] and Fawzy and Hougen[30] have developed a formalism for handling the electronic and spin angular momenta in near-rigid open-shell complexes; this has been used to analyze the microwave and radiofrequency spectrum of Ar–NO (Ref. 31) and to obtain information on the potential energy surfaces for Ar–NO and Ne–NO.[32]

The purpose of the present paper is to investigate the spectra of atom–open-shell diatom complexes from a more general viewpoint, in order to understand the structure of the energy levels involved. The angular momentum algebra involved is similar to that needed in considering the scattering of open-shell diatoms from atoms,[33–41] but the physical consequences are different for bound states. We will pay particular attention to the way in which the anisotropy of the potential mixes the free-rotor levels of the diatomic fragment, and to the way the free-rotor levels correlate with those of a semirigid triatomic molecule as the anisotropy is increased. We will discuss complexes formed from diatomic molecules in both Σ and Π states. Although Ar–OH and Ne–OH will be considered as examples, the discussion is general, and may be applied equally well to complexes containing species such as CH, CN, NO, and O_2.

II. MONOMER ENERGY LEVELS

The rotational energy levels and wave functions of open-shell diatomic molecules are well understood, but will be described briefly here in order to set the scene and define the notation used. In keeping with the usual convention for Van der Waals complexes, we use lower-case letters to identify quantities (and quantum numbers) that relate to monomers, and reserve upper-case letters to describe properties of the complex as a whole.

Within the Born–Oppenheimer approximation, the electronic, vibrational, and rotational motions may be considered separately. In this paper we will not consider the diatom stretching motion, since the coupling of different diatom vibrational states by the intermolecular potential does not give rise to qualitative spectroscopic effects. If nuclear spin is neglected, there are three possible sources of angular momentum in a diatomic molecule: **l**, the total orbital angular momentum of the electrons; **s**, the total spin angular momentum of the electrons; and **r**, the rotational angular momentum of the nuclei. For the cases we will consider here, the orbital angular momentum **l** is strongly coupled to the internuclear axis, with projection λ.

To a first approximation, the monomer Hamiltonian can be written as a sum of electrostatic, rotational, spin–orbit

 0021-9606/91/127602-17$03.00

coupling and spin–rotation coupling terms,

$$H_{\rm mon} = H_{\rm elec} + H_{\rm rot} + H_{\rm so} + H_{\rm sr} = H_{\rm elec} + b\hat{\mathbf{r}}^2 + a\hat{\mathbf{l}}\cdot\hat{\mathbf{s}} + H_{\rm sr}, \quad (1)$$

where $H_{\rm elec}$ is the electrostatic Hamiltonian for the electron motions, b is the monomer rotational constant, and a is the spin–orbit coupling constant. The spin–rotation term $H_{\rm sr}$ includes any spin–spin coupling terms. The type of angular momentum coupling observed depends on the relative sizes of the first three terms. The most common case is Hund's case (a), which arises when the spin–orbit coupling is large compared to $H_{\rm rot}$ but small compared to the splitting between states of different λ; this is the case for most Π state monomers. Under these circumstances, the spin–orbit interaction results in **s** being strongly coupled to λ and hence to the internuclear axis; **s** then has a well-defined projection quantum number σ. The vector **r** is perpendicular to the internuclear axis, so the projection of the total angular momentum **j** onto the axis is $\omega = \lambda + \sigma$. In a $^2\Pi$ state, for example, we have $\lambda = \pm 1$, $\sigma = \pm\frac{1}{2}$, and $\omega = \pm\frac{1}{2}$ or $\pm\frac{3}{2}$; note that in the present work we take λ, σ, and ω to be signed quantum numbers, not moduli.

Hund's case (b) coupling arises if the spin–orbit interaction is small compared to $H_{\rm rot}$ (more specifically, $H_{\rm so} < bj$). This is the usual situation for Σ states, where there is no first-order spin–orbit interaction, and also arises for high rotational levels of some Π states. Under these circumstances **l** but not **s** is quantised along the internuclear axis; **r** and λ couple to form a resultant **n**, which then couples with **s** to form a resultant **j**. Both **n** and **j** are good quantum numbers, but ω is not. Levels of the same r but different j are split by spin–rotation coupling (see below), which is usually small compared to the splitting between levels of different r.

Hund's case (c) arises when the spin–orbit coupling is large compared to the interaction coupling **l** to the internuclear axis. Under these circumstances **l** and **s** couple to form a resultant $\mathbf{j}_a$, with projection ω on the internuclear axis; since **r** is perpendicular to the axis, ω is also the projection of the total angular momentum **j**. For case (c), neither λ nor σ is individually well defined. We will not deal explicitly with case (c) diatomic molecules in the present paper, but it nevertheless provides a useful analogy for the coupling cases described below for open-shell Van der Waals complexes.

The energy level schemes are thus quite different for diatomic molecules in Σ and Π states. For Σ states $H_{\rm so}$ has no effect in first order. The spin–rotation Hamiltonian is different for $^2\Sigma$ and $^3\Sigma$ states: for $^2\Sigma$ states it is just $H_{\rm sr} = \gamma\hat{\mathbf{r}}\cdot\hat{\mathbf{s}}$, and the energy levels are

$$E(^2\Sigma,rj) = br(r+1) + \tfrac{1}{2}\gamma[j(j+1) - r(r+1) - s(s+1)]. \quad (2)$$

The spin– rotation constant γ is usually very small, so that for $^2\Sigma$ states the dominant term is the rotational term $br(r+1)$. For $^3\Sigma$ states, however, there is a substantial contribution to $H_{\rm sr}$ arising from spin–spin coupling, which may be comparable to the rotational term: in O_2 $^3\Sigma_g^-$, for example, the spin–spin coupling constant of 1.98 $\rm cm^{-1}$ may be compared with the rotational constant $b = 1.44$ $\rm cm^{-1}$.

For Π states exhibiting case (a) coupling, the monomer wave function may be written as a product of an electronic part and a rotational part. If $H_{\rm sr}$ is neglected, the Hamiltonian becomes

$$H_{\rm mon} = b\left[\hat{\mathbf{j}}^2 + \hat{\mathbf{s}}^2 - \hat{s}_z^2 - \hat{j}_z^2 + \frac{a}{b}\hat{l}_z\hat{s}_z\right] + \left(b + \frac{1}{2}a\right)(\hat{l}_+\hat{s}_- + \hat{l}_-\hat{s}_+) + b[(\hat{l}_+\hat{l}_- + \hat{l}_-\hat{l}_+) - \hat{j}_+(\hat{l}_- + \hat{s}_-) - \hat{j}_-(\hat{l}_+ + \hat{s}_+)]. \quad (3)$$

The first-order energy level expressions for Π states of various kinds may then be found by applying the diagonal part of the Hamiltonian,

$$\begin{aligned} E(^1\Pi_1 j) &= bj(j+1) - b, \\ E(^2\Pi_{1/2} j) &= bj(j+1) + \tfrac{1}{4}b - \tfrac{1}{2}a, \\ E(^2\Pi_{3/2} j) &= bj(j+1) - \tfrac{7}{4}b + \tfrac{1}{2}a, \\ E(^3\Pi_0 j) &= bj(j+1) - b - a, \\ E(^3\Pi_1 j) &= bj(j+1) - b, \\ E(^3\Pi_2 j) &= bj(j+1) - 3b + a. \end{aligned} \quad (4)$$

For open-shell diatomic monomers it is usual to consider states with definite parity p. For case (b) coupling with $\lambda \neq 0$, it is necessary to consider linear combinations of corresponding states with positive and negative λ: states given by

$$|\lambda^{\eta}, n, j\rangle = |+\lambda, n, j\rangle + \eta|-\lambda, n, j\rangle \quad (5)$$

with $\eta = \pm 1$ have parity $p = \eta(-1)^n$. Similarly, for case (a), it is necessary to consider linear combinations of corresponding states with positive and negative ω: states given by

$$|\lambda\,{}^{\epsilon}_{\omega} j\rangle = |+\lambda_{+\omega} j\rangle + \epsilon|-\lambda_{-\omega} j\rangle \quad (6)$$

have parity $p = \epsilon(-1)^{j-s}$. The states with $\epsilon = +1$ and -1 are designated e and f, respectively, and are degenerate in this approximation. However, as will be seen below, for Van der Waals complexes it is advantageous to use a basis set of states with signed projection quantum numbers instead of considering definite parity states at this stage; this is permissible because the inversion operation for the *monomer* is not a symmetry operation of the *complex*.

It should be noted that deviations from case (a) coupling are often important, especially for diatomic hydrides. The $b(\hat{j}_-\hat{s}_+ + \hat{j}_+\hat{s}_-)$ part of the Hamiltonian (3) couples states with $\Delta\sigma = \pm 1$ and hence $\Delta\omega = \pm 1$, and causes significant mixing unless bj is much smaller than a; for large b or j, this mixing causes a changeover to case (b) coupling. For OH $X\,^2\Pi$ with $j = \frac{5}{2}$, for example, the energy levels are shifted by about 15 $\rm cm^{-1}$ from the pure case (a) predictions by the rotational decoupling. In addition, the last parts of the Hamiltonian, $(\hat{j}_+\hat{l}_- + \hat{j}_-\hat{l}_+)$ and $(\hat{l}_+\hat{s}_- + \hat{l}_-\hat{s}_+)$, couple different electronic states. The Π–Σ interaction is different for e and f monomer levels, and gives rise to λ doubling in Π states.

III. ANGULAR MOMENTUM COUPLING CASES FOR VAN DER WAALS COMPLEXES

A. Closed-shell Van der Waals complexes

The coupling cases appropriate for closed-shell Van der Waals complexes have been the subject of a good deal of work; they were originally introduced by Bratoz and Martin,[42] and have recently been reviewed by Hutson.[43] The notation used in the present paper is close to that of Ref. 43. Except for very weakly anisotropic systems, such as Ar–H_2, the energy levels of closed-shell complexes are best described by body-fixed (case 2 or 3) coupling, in which the diatom rotational angular momentum **j** is quantised along the intermolecular axis with projection K; the end-over-end rotational angular momentum of the complex, **L**, is perpendicular to the intermolecular vector, so that K is also the projection of the total angular momentum **J**. The total wave function (neglecting vibrations of the diatom) may be written

$$\psi = R^{-1}\sum_{jK} \Phi_{jK}^{JM}\chi_{jK}^{JM}(R). \tag{7}$$

The angular functions Φ_{jK}^{JM} are

$$\Phi_{jK}^{JM} = \left(\frac{2J+1}{4\pi}\right)^{1/2} \mathscr{D}^{J*}_{MK}(\alpha,\beta,0)\, Y_{jK}(\theta,\phi), \tag{8}$$

where $\mathscr{D}^{J}_{MK}(\alpha,\beta,0)$ is a rotation matrix describing the orientation of the intermolecular vector **R** in space and $Y_{jK}(\theta,\phi)$ is a spherical harmonic describing the orientation of the diatom in the body-fixed axis system, which is obtained from the space-fixed system by rotating through angles α and β. If the intermolecular potential is expanded in Legendre polynomials,

$$V_{\text{inter}} = \sum_l P_l(\cos\theta)\, V_l(R), \tag{9}$$

the potential matrix elements between the angular basis functions may be written

$$\langle JM;jK\,|\,V_{\text{inter}}\,|\,JM;j'K'\rangle = \delta_{KK'}\sum_l V_l(R) g_l(jj'K), \tag{10}$$

where the potential coupling coefficients $g_l(jj'K)$ are

$$\begin{aligned} g_l(jj'K) &\equiv \langle jK\,|P_l(\cos\theta)\,|j'K\rangle \\ &= (-1)^K[(2j+1)(2j'+1)]^{1/2} \\ &\quad\times \begin{pmatrix} j & l & j' \\ 0 & 0 & 0 \end{pmatrix}\begin{pmatrix} j & l & j' \\ -K & 0 & K \end{pmatrix}. \end{aligned} \tag{11}$$

The dynamics of such complexes and the correlation diagrams observed as a function of increasing anisotropy have been investigated in detail in Ref. 43. If Coriolis coupling is neglected, the good quantum numbers for low anisotropies are j, J, and K; J and K remain good quantum numbers as the anisotropy is increased, but j is replaced by a bending quantum number.

B. Open-shell Van der Waals complexes

The Hamiltonian for an atom–open shell diatom system may be written in body-fixed coordinates,

$$H = \frac{\hbar^2}{2\mu}\left[-R^{-1}\frac{\partial^2}{\partial R^2}R + \frac{(\hat{\mathbf{J}}-\hat{\mathbf{j}})^2}{R^2}\right] + H_{\text{mon}} + V_{\text{inter}}, \tag{12}$$

where R is the intermolecular distance, μ is the collision reduced mass, $\hat{\mathbf{J}}$ is the total angular momentum operator for the complex, and V_{inter} is the intermolecular potential. This is similar to the corresponding Hamiltonian for a complex involving a closed-shell diatom,[43] except that the monomer angular momentum operator $\hat{\mathbf{j}}$ takes a more complicated form.

The intermolecular potential for interaction of an open-shell diatom with an atom is independent of spin, and its matrix elements between electronic states may be written

$$V_{\lambda\lambda'}(R,\theta) = \int \psi_\lambda^{s*} V_{\text{inter}} \psi_{\lambda'}^{s}\, d\tau. \tag{13}$$

The potential energy surfaces $V_{\lambda\lambda'}(R,\theta)$ may be expanded in rotation matrices (or, equivalently, renormalized spherical harmonics)

$$\begin{aligned} V_{\lambda\lambda'}(R,\theta) &= \sum_l \mathscr{D}^{l*}_{0,\lambda-\lambda'}(0,\theta,0)\, V_{l,\lambda-\lambda'}(R) \\ &= \sum_l C_l^{\lambda-\lambda'}(\theta,0)\, V_{l,\lambda-\lambda'}(R). \end{aligned} \tag{14}$$

Thus for Σ states the expansion of the electronically diagonal part of the potential includes only V_{l0} terms, whereas for Π states there are additional V_{l2} terms for $l \geqslant 2$.

1. Complexes of monomers in Σ states

In a complex formed from a multiplet Σ diatom, there are three sources of angular momentum: $\mathbf{r}\equiv\mathbf{n}$, the angular momentum of the diatom excluding spin; **s**, the electron spin angular momentum; and **L**, the pseudodiatomic rotational angular momentum of the complex as a whole. Several different coupling schemes for these angular momenta may be envisaged: they are closely analogous to Hund's coupling cases, and will be referred to as cases (A), (B), and (C). The vector coupling diagrams for the different coupling cases, and the analogy to Hund's coupling cases, are shown in Fig. 1. The coupling case appropriate to a particular complex will be governed by the relative magnitudes of V_{inter} (which plays the role of H_{elec}), H_{sr} (which plays the role of H_{so}), and $B(\hat{\mathbf{J}}-\hat{\mathbf{j}})^2$ (which plays the role of H_{rot}); B is the rotational constant of the complex. Most real complexes of $^2\Sigma$ diatoms will follow case (B) coupling, while those of $^3\Sigma$ diatoms may follow case (A) coupling if $H_{\text{sr}} > BJ$. As for diatomic molecules, case (A) complexes may exhibit a changeover to case (B) coupling with increasing J. Case (C) coupling will occur only if H_{sr} is large compared to the potential anisotropy, which is unlikely.

Case (A)

In case (A), **r** and **s** are each strongly coupled to the inter*molecular* axis, with projections $\mathscr{R}$ and Σ respectively. The vector **L** is perpendicular to the intermolecular axis, so the projection of the total angular momentum **J** onto the axis is $P = \mathscr{R} + \Sigma$. This is the coupling scheme described by Van der Avoird[44] for rare gas–O_2 complexes. The most appropriate functions for expanding the total wave function are those

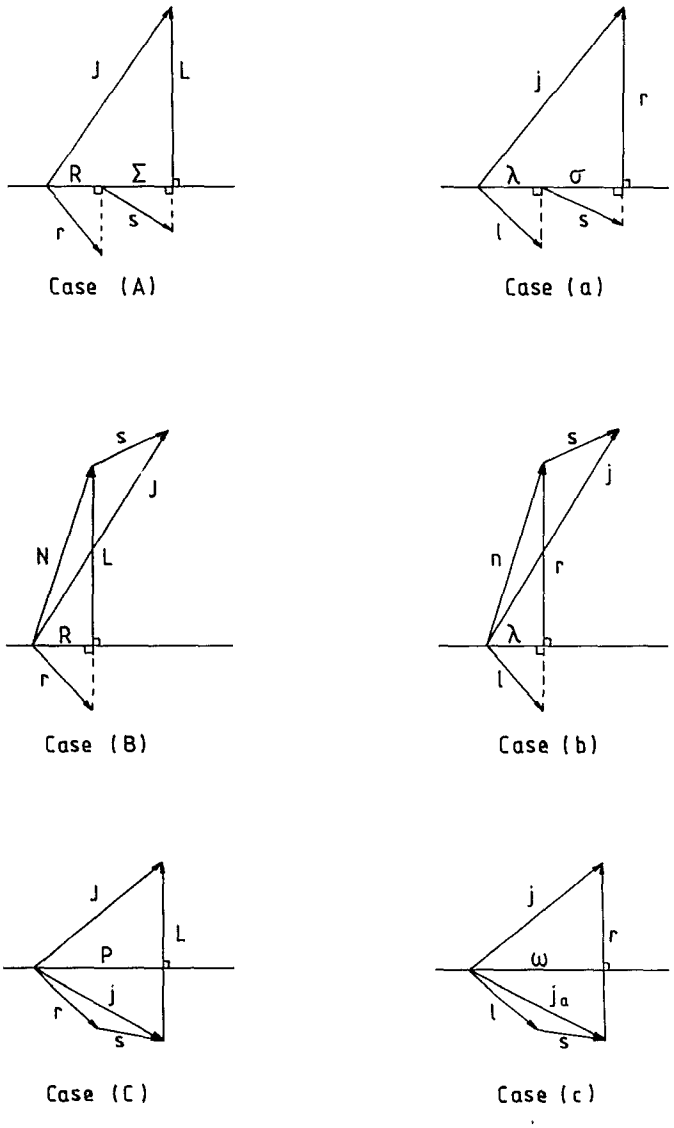

FIG. 1. Vector diagrams showing the relationship between the coupling cases [(A), (B), and (C)] that may arise for complexes formed from multiplet Σ diatoms and the analogous Hund's coupling cases [(a), (b), and (c)] for diatomic molecules.

that give the most nearly diagonal Hamiltonian matrix. For case (A), neglecting vibrations of the diatom, the best expansion is

$$\psi = R^{-1} \sum_{r,\mathscr{R},\Sigma} \Phi^{JMs}_{r,\mathscr{R},\Sigma} \chi^{JMs}_{r,\mathscr{R},\Sigma}(R), \tag{15}$$

where the angular functions $\Phi^{JMs}_{r,\mathscr{R},\Sigma}$ are

$$\Phi^{JMs}_{r,\mathscr{R},\Sigma} = \left(\frac{2J+1}{4\pi}\right)^{1/2} \mathscr{D}^{J*}_{MP}(\alpha,\beta,0)\, Y_{r\mathscr{R}}(\theta,\phi)\, \psi_{s\Sigma}. \tag{16}$$

Since the intermolecular potential is independent of spin, the potential matrix elements between the angular basis functions may be written

$$\langle JM;r\mathscr{R};s\Sigma|V_{\text{inter}}|JM;r'\mathscr{R}';s'\Sigma'\rangle$$

$$= \delta_{ss'}\delta_{\Sigma\Sigma'}\delta_{\mathscr{R},\mathscr{R}'} \sum_l V_l(R) g_l(rr'\mathscr{R}), \tag{17}$$

where the potential coupling coefficients $g_l(rr'\mathscr{R})$ are

$$g_l(rr'\mathscr{R}) \equiv \langle r\mathscr{R}|C^0_l|r'\mathscr{R}\rangle = (-1)^{\mathscr{R}}[(2r+1)(2r'+1)]^{1/2} \times \begin{pmatrix} r & l & r' \\ 0 & 0 & 0 \end{pmatrix} \begin{pmatrix} r & 1 & r' \\ -\mathscr{R} & 0 & \mathscr{R} \end{pmatrix}. \tag{18}$$

These are exactly the same as the corresponding coefficients (11) for the case of a closed-shell ($^1\Sigma$) diatom, except that r and $\mathscr{R}$ appear in place of j and K.

In a complete treatment, including the effects of overall rotation of the complex, linear combinations of the angular functions of Eq. (16) with definite (total) parity must be considered. The functions

$$\Phi^{JMs}_{r\mathscr{R}\Sigma} + \xi \Phi^{JMs}_{r,-\mathscr{R},-\Sigma}, \tag{19}$$

with $\xi = \pm 1$, have parity $\xi(-1)^{J-s}$.

Case (B)

In case (B), **r** but not **s** is quantised along the intermolecular axis; **r** again has a well-defined projection quantum number $\mathscr{R}$. **L** and $\mathscr{R}$ couple to form a resultant **N**, which then couples with **s** to form a resultant **J**. Both **N** and **J** are good quantum numbers, but P is not. The basic difference from case (A) is that N replaces Σ as a good quantum number. The total wave function for a case (B) complex is most appropriately expanded

$$\psi = R^{-1} \sum_{rN\mathscr{R}} \Phi^{JMs}_{rN\mathscr{R}} \chi^{JMs}_{rN\mathscr{R}}(R), \tag{20}$$

where the angular functions $\Phi^{JMs}_{rN\mathscr{R}}$ are

$$\Phi^{JMs}_{rN\mathscr{R}} = \sum_{M_N M_s} \langle NM_N sM_s|JM\rangle \times \left[\left(\frac{2N+1}{4\pi}\right)^{1/2} \mathscr{D}^{N*}_{M_N\mathscr{R}}(\alpha,\beta,0)\, Y_{r\mathscr{R}}(\theta,\phi)\right] \psi_{sM_s}. \tag{21}$$

The potential matrix elements between the angular basis functions are

$$\langle JM;rN\mathscr{R}s|V_{\text{inter}}|JM;r'N'\mathscr{R}'s'\rangle$$

$$= \delta_{NN'}\delta_{\mathscr{R},\mathscr{R}'}\delta_{ss'} \sum_l V_l(R) g_l(rr'\mathscr{R}), \tag{22}$$

where the potential coupling coefficients are the same as for case (A), Eq. (18).

The definite parity functions for a case (B) complex are of the form

$$\Phi^{JMs}_{rN\mathscr{R}} + \zeta \Phi^{JMs}_{rN,-\mathscr{R}}, \tag{23}$$

with $\zeta = \pm 1$, and have parity $\zeta(-1)^N$.

Case (C)

In case (C), **r** and **s** first couple together to form a resultant **j** (as in the free diatom); **j** is then quantised along the intermolecular axis with projection P. Since **L** has no projection onto the intermolecular axis, P is also the projection of the total angular momentum **J**. For case (C), neither $\mathscr{R}$ nor Σ is individually well defined. The total wave function is most appropriately expanded

$$\psi = R^{-1} \sum_{rjP} \Phi^{JMs}_{rjP} \chi^{JMs}_{rjP}(R), \tag{24}$$

where the angular functions Φ^{JMs}_{rjP} are

$$\Phi_{rjP}^{JMs} = \left(\frac{2J+1}{4\pi}\right)^{1/2} \mathscr{D}_{MP}^{J*}(\alpha,\beta,0) \times \sum_{m_r m_s} \langle rm_r sm_s | jP\rangle \left(\frac{2r+1}{4\pi}\right)^{1/2} \mathscr{D}_{m_r,0}^{r*}(\phi,\theta,0)\psi_{m_s}^{s}. \quad (25)$$

The potential matrix elements between the angular basis functions may be obtained from the Wigner–Eckart theorem[45]

$$\langle JM;rsjP|V_{\text{inter}}|JM;r's'j'P'\rangle = \delta_{PP'}\delta_{ss'}\sum_l V_l(R) g_{ls}(rr'jj'P), \quad (26)$$

where the potential coupling coefficients $g_{ls}(rr'jj'P)$ are

$$g_{ls}(rr'jj'P) \equiv \langle rsjPJ|C_l^0|r'sj'PJ\rangle = (-1)^{l+s+j+j'-P} \times [(2r+1)(2r'+1)(2j+1)(2j'+1)]^{1/2} \times \begin{Bmatrix} j & j' & l \\ r' & r & s \end{Bmatrix} \begin{pmatrix} r & l & r' \\ 0 & 0 & 0 \end{pmatrix} \begin{pmatrix} j & l & j' \\ -P & 0 & P \end{pmatrix}. \quad (27)$$

These again reduce to the coupling coefficients for the $^1\Sigma$ case for $s = 0$.

2. Complexes of monomers in Π states

For monomers following Hund's case (a) there are fewer possibilities, because (for low values of j) the monomer spin–orbit interaction causes **l** and **s** to remain coupled to the *monomer* internuclear axis even in the complex. The most appropriate expansion for the total wave function is therefore

$$\psi = R^{-1}\sum_{jP\lambda\sigma} \Phi_{jP,\lambda\sigma}^{JMs}\chi_{jP,\lambda\sigma}^{JMs}(R), \quad (28)$$

where the angular functions $\Phi_{jP,\lambda\sigma}^{JMs}$ are

$$\Phi_{jP,\lambda\sigma}^{JMs} = \left(\frac{2J+1}{4\pi}\right)^{1/2} \mathscr{D}_{MP}^{J*}(\alpha,\beta,0) \times \left(\frac{2j+1}{4\pi}\right)^{1/2} \mathscr{D}_{P\omega}^{j*}(\phi,\theta,0)\psi_{s\sigma}\psi_{\lambda} \quad (29)$$

and $\omega = \lambda + \sigma$ as for the free monomer.

The potential matrix elements between the angular basis functions may be written

$$\langle JM;jP\lambda s\sigma|V_{\text{inter}}|JM;j'P'\lambda's'\sigma'\rangle = \delta_{ss'}\delta_{\sigma\sigma'}\delta_{PP'}\sum_l V_{l,\lambda-\lambda'}(R) g_{l,\lambda-\lambda'}(j\omega j'\omega' P), \quad (30)$$

where the potential coupling coefficients $g_{l,\lambda-\lambda'}(j\omega j'\omega' P)$ are

$$gl(rr'\mathscr{R}) \equiv \langle j\omega PJ|C_l^{\lambda-\lambda'}|j'\omega' PJ\rangle = (-1)^{P-\omega}[(2j+1)(2j'+1)]^{1/2} \times \begin{pmatrix} j & l & j' \\ -\omega & \lambda-\lambda' & \omega' \end{pmatrix} \begin{pmatrix} j & l & j' \\ -P & 0 & P \end{pmatrix}. \quad (31)$$

These are similar to the corresponding coefficients (11) for the case of a closed-shell diatom, except for the phase factor and the fact that the first 3-j symbol has projections involving ω and λ instead of zero.

In a complete treatment, including the effects of overall rotation of the complex, it is again necessary to consider linear combinations of the angular functions with definite (total) parity. As will be seen below, states with different relative signs of ω and P are not usually degenerate, so the appropriate linear combinations are

$$\Phi_{jP,\lambda\sigma}^{JMs} + \xi\Phi_{j,-P,-\lambda,-\sigma}^{JMs}, \quad (32)$$

with $\xi = \pm 1$, and have parity $\xi(-1)^{J-s}$. Note that the parity operator changes the signs of both P and ω $(=\lambda+\sigma)$ simultaneously.

IV. ENERGY LEVELS FOR BENDING MOTIONS

For any of the coupling cases, the expressions obtained above may be substituted into the total Schrödinger equation to obtain a set of coupled differential equations, which may then be solved either directly or using a basis set expansion for the R coordinate.[43] However, a good deal of insight may be obtained by considering the bending motion separately, and we shall consider this approximation first. If the intermolecular stretching motion and the overall rotation of the complex are neglected, the resulting Hamiltonian for bending (hindered rotational) motion is

$$H_{\text{bend}} = H_{\text{mon}} + V. \quad (33)$$

We therefore consider the model bending Hamiltonians,

$$H_{\text{bend}}^{(0)} = E^0 + br(r+1) + V_{10}C_1^0(\theta,0) + V_{20}C_2^0(\theta,0) \quad \text{(for } \Sigma \text{ states)}, \quad (34)$$

$$H_{\text{bend}}^{(0)} = E^0 + bj(j+1) + V_{10}C_1^0(\theta,0) + V_{20}C_2^0(\theta,0) \quad \text{(for } \Pi \text{ states)}, \quad (35)$$

where V_{10} and V_{20} are the (radially averaged) effective anisotropies.

Note that the model Hamiltonians do not include the end-over-end rotation of the complex. They thus omit the $\hat{\mathbf{j}}\cdot\hat{\mathbf{J}}$ term from the true Hamiltonian, and therefore neglect the coupling between states of different $\mathscr{R}$ (for Σ states) or P (for Π states). Omitting the overall rotation allows us to show correlation diagrams that scale solely with the diatom rotational constant b and can thus be applied to any open-shell atom–diatom complex. In a more complete treatment, with overall rotation included, the eigenstates of the complex have definite parity, and are formed by taking linear combinations of corresponding states with positive and negative $\mathscr{R}$ or P as in Eqs. (19), (23), and (32). The degeneracy of the + and − parity states is lifted by off-diagonal matrix elements of the $\hat{\mathbf{j}}\cdot\hat{\mathbf{J}}$ term in the Hamiltonian, producing P-type doubling in the complex.

A. Correlation diagrams for Σ state monomers

As discussed above, the body-fixed coupling coefficients for case (A) and (B) complexes of Σ state diatomic molecules are closely isomorphic to those for closed-shell systems. The eigenvalues of the model Hamiltonian (34) have been evaluated as a function of V_{20} for various values of V_{10}, and sample results are shown as correlation diagrams in Fig.

2. Figure 2(a) shows the results for a homonuclear diatom (with $V_{10} = 0$), and Fig. 2(b) the results for a heteronuclear diatom with $V_{10} = 2b$. Figures 2(c) and 2(d) show expanded versions of the central portions of Figs. 2(a) and 2(b), respectively. All energies are scaled according to b, the diatom rotational constant. In each diagram the left-hand side corresponds to large negative V_{20}, i.e., a near-rigid complex with a linear equilibrium geometry, while the right-hand side corresponds to large positive V_{20}, i.e., a near-rigid complex with a T-shaped geometry. The anisotropies near these limits are probably unrealistically high for diatomic molecules in their electronic ground states, but it should be remembered that the potential energy surfaces for electronically excited states may be much more strongly bound and anisotropic because of exciplex formation.

For small anisotropies ($V_{20} \leqslant b$), there is little difference between Figs. 2(c) and 2(d) because the V_{10} anisotropy has no diagonal matrix elements between the case (A) or case (B) basis functions. The energy levels in this region are dominated by the V_{20} anisotropy. The energy levels of weak-anisotropy complexes of this type should be described by quantum numbers r, $\mathscr{R}$, J, s, and either Σ [for case (A)] or N [for case (B)]. As the anisotropy is increased, r becomes poorly defined but $\mathscr{R}$ is nearly conserved (except for Coriolis coupling effects arising from the overall rotation).

The figures do not show the effects of either overall rotation or electron spin; the levels shown are characterized by a good quantum number $\mathscr{R}$, and rotational and spin ladders may be built upon each level. The principal differences between case (A) and case (B) arise in the way in which this is done. For case (A) the spin is introduced first, and its projection number Σ onto the intermolecular axis is well-defined: the states are characterized by a nearly good quantum number $P = \mathscr{R} + \Sigma$, and each P state supports a rotational ladder with $J \geqslant P$. For case (B), by contrast, the overall rotation is introduced first: each $\mathscr{R}$ level supports a rotational ladder with $N \geqslant \mathscr{R}$, and the spin is introduced last, splitting each N state into $2s + 1$ components with different values of J. As mentioned above, case (A) complexes may exhibit a changeover to case (B) with increasing rotational quantum number.

It is interesting to consider the way that the energy levels behave in the large-anisotropy limits. For large negative V_{20} the energy levels are those of a linear triatomic molecule: there is a bending quantum number v_2 and a vibrational angular momentum l which runs from $-v_2$ to $+v_2$ in steps of 2. The states are described by $\mathscr{R} \equiv l$ (with additional splittings as described above). In the homonuclear case the wells at $\theta = 0$ and $\theta = 180°$ are of equal depth, so all the bending vibrational levels are doubled; the tunnelling splitting becomes zero as $V_{20} \rightarrow -\infty$. In the heteronuclear case the wells at $\theta = 0$ and $\theta = 180°$ are different, so each well gives rise to a set of equally spaced bending levels; the two sets have origins differing by $2V_{10}$ and slightly different vibrational spacings. If V_{10} is large enough that the complex has a linear equilibrium geometry, the energy level pattern will be the same as on the left-hand side of Fig. 2(a) but without the tunnelling doubling, as discussed in Ref. 43.

For large positive V_{20} the energy levels are those of a nonlinear triatomic molecule. The energy levels will in general be those of a near-symmetric prolate top, possibly with the added complication of electron spin. The levels are characterized by a (nondegenerate) bending quantum number v, and a nuclear rotational angular momentum with a projection $K_A \equiv \mathscr{R}$ onto the intermolecular axis. For $V_{10} = 0$, the A rotational constant of the complex is equal to the diatom rotational constant b. The principal effect of a V_{10} anisotropy is to tip the equilibrium geometry away from $\theta = 90°$, so that the A rotational constant of the complex is no longer the same as b. However, the value of V_{10} used in Figs. 2(b) and 2(d) is not large enough to show this effect to any significant extent.

For monomers in multiplet Σ states the possibility of either case (A) or case (B) coupling persists for high values of V_{20}, with Σ or N respectively as a nearly good quantum number.

B. Correlation diagrams for Π state monomers

A similar analysis may be performed for Π state monomers, using the matrix elements of Eq. (31), and the results are shown in Figs 3–6 for $^1\Pi_1$, $^2\Pi_{1/2}$, $^2\Pi_{3/2}$, and $^3\Pi_2$ monomers, respectively. If the V_{22} potential term is omitted, only ω and not λ is present in Eq. (31), so that the correlation diagrams for $^3\Pi_0$ monomers are the same as for Σ state monomers (Fig. 2) and those for $^3\Pi_1$ monomers are the same as for $^1\Pi_1$ monomers (Fig. 3).

One qualitative difference from the Σ state case arises immediately whenever $\omega \neq 0$. For diatoms in Σ states, the first 3-j symbol in Eq. (11) or Eq. (18) is zero if $j = j'$ (or $r = r'$) and l is odd, so that V_{10} has no diagonal matrix elements in the free-rotor limit. However, if ω and P are nonzero, this is no longer true in Eq. (31). For diatoms with $\omega \neq 0$ the V_{10} anisotropy shifts the $+\omega$ and $-\omega$ states for a given P by equal and opposite amounts, so that $|JjP + \omega\rangle$ and $|JjP - \omega\rangle$ are no longer near-degenerate. Thus for weakly anisotropic Van der Waals complexes involving heteronuclear diatomic molecules in Π states (such as the ground electronic state of Ar–OH) it is convenient to consider primitive diatom functions with signed ω quantum numbers instead of parity-adapted states with $\epsilon = \pm 1$. However, it is still necessary to consider the total parity of the complex as in Eq. 32: the $\hat{\mathbf{j}}\cdot\hat{\mathbf{J}}$ term in the total Hamiltonian will produce P-type doubling in the complex in exactly the same way as for l-type doubling in closed-shell systems.

A slightly different way of viewing the effect of V_{10} is to realize that the internal rotational functions of Eq. (29) for diatoms with $\omega \neq 0$ are rotation matrices rather than spherical harmonics, and that rotation matrices (unlike spherical harmonics) are not necessarily either symmetric or antisymmetric with respect to the transformation $\theta \rightarrow \pi - \theta$. The free-rotor probability density functions

$$(j + \tfrac{1}{2})\left[d^j_{P\omega}(\theta)\right]^2 \tag{36}$$

are shown for a variety of values of j, P, and ω in Fig. 7. Even in the free-rotor limit, monomers with $\omega \neq 0$ may preferentially have one end or the other nearest the atom: if the intermolecular potential is deeper at one end than the other, this will lift the degeneracy of the states with $\pm\omega$.

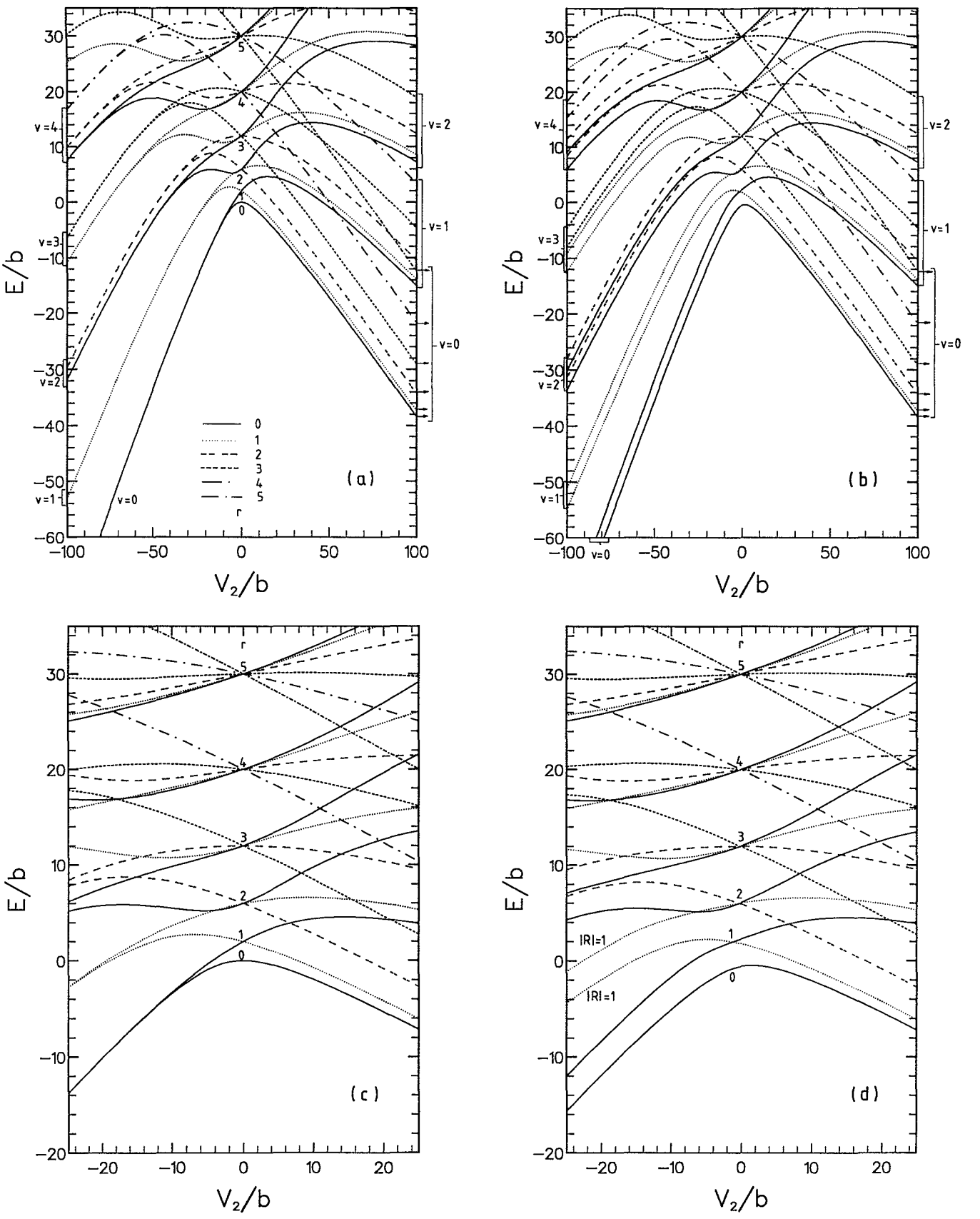

FIG. 2. Correlation diagrams for complexes containing diatoms in Σ states. Parts (a) and (b) show the bending energy levels as a function of the V_{20} anisotropy for $V_{10} = 0$ and $2b$ respectively. Large negative V_{20} corresponds to a near-rigid complex with a linear equilibrium geometry, large positive V_{20} corresponds to a near-rigid complex with a T-shaped geometry, and $V_{20} = 0$ corresponds to a free internal rotor. States with different values of the projection quantum number $\mathscr{R}$ are shown with different line types as indicated in part (a). Parts (c) and (d) show expanded versions of the central regions of parts (a) and (b), respectively. All energies are shown in terms of the monomer rotational constant b.

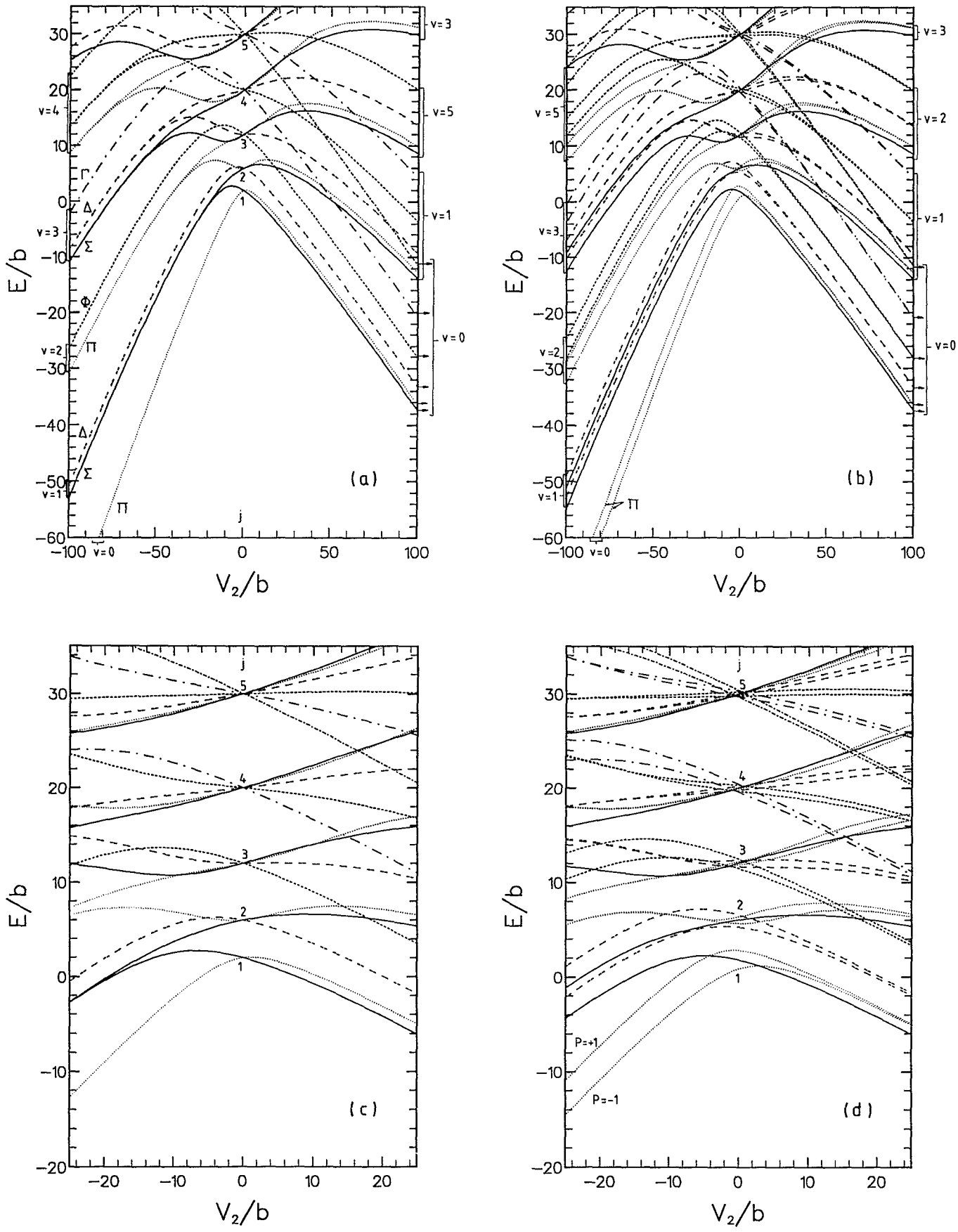

FIG. 3. Correlation diagrams for complexes containing diatoms in $^1\Pi$ or $^3\Pi$ states. Parts (a) and (b) show the bending energy levels as a function of the V_{20} anisotropy for $V_{10} = 0$ and $2b$ respectively. States with different values of the projection quantum number $P \equiv K$ are shown with different line types as indicated in Fig. 2(a). In the near-rigid linear limit, the states are given vibronic labels Σ, Π, Δ, etc. indicating the value of K. Parts (c) and (d) show expanded versions of the central regions of parts (a) and (b), respectively. All energies are shown in terms of the monomer rotational constant b.

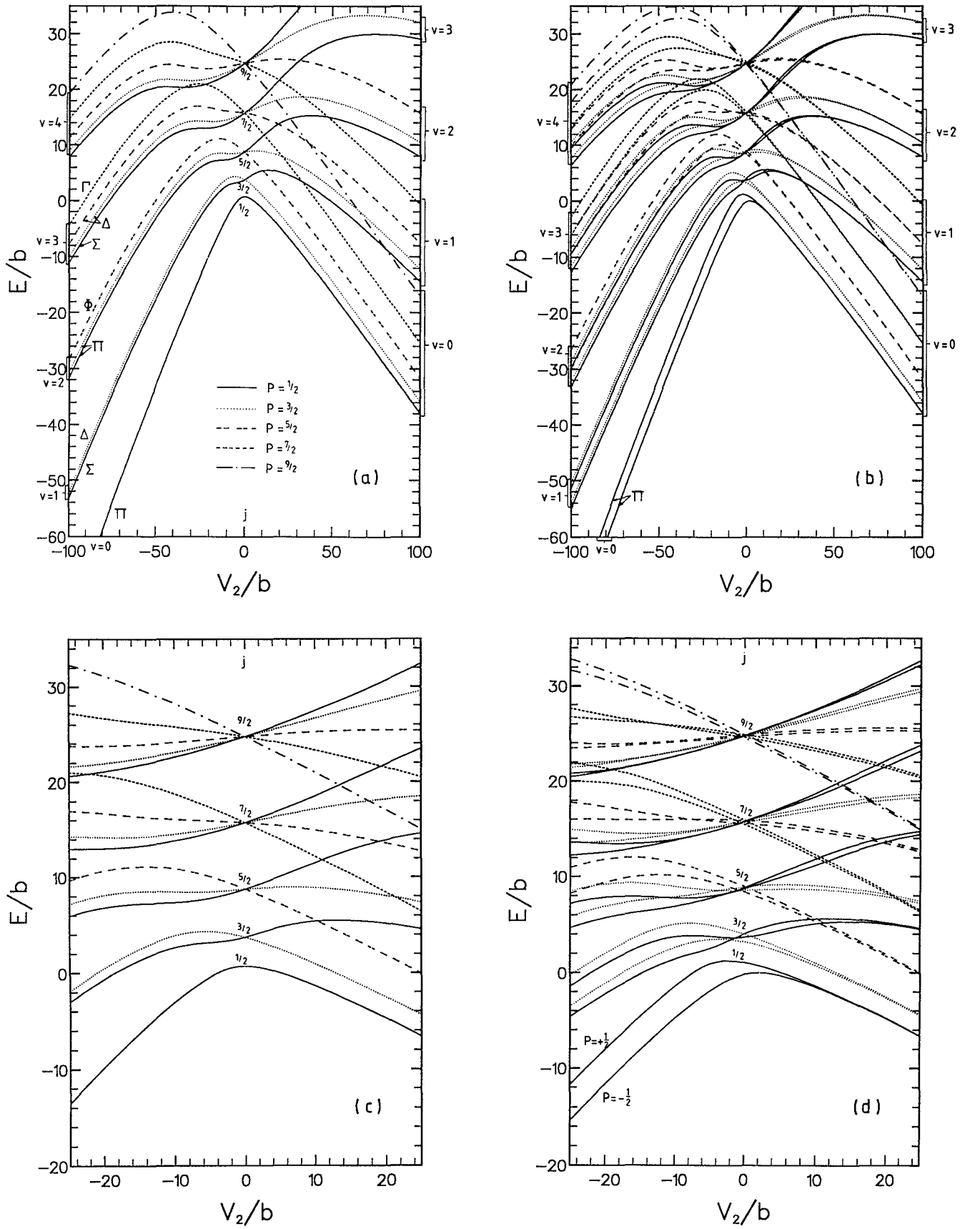

FIG. 4. Correlation diagrams for complexes containing diatoms in $^2\Pi_{1/2}$ states. Parts (a) and (b) show the bending energy levels as a function of the V_{20} anisotropy for $V_{10} = 0$ and $2b$, respectively. States with different values of the projection quantum number P are shown with different *line types* as indicated in part (a). In the near-rigid linear limit, the states are given vibronic labels indicating the value of K. Parts (c) and (d) show expanded versions of the central regions of parts (a) and (b), respectively. All energies are shown in terms of the monomer rotational constant b.

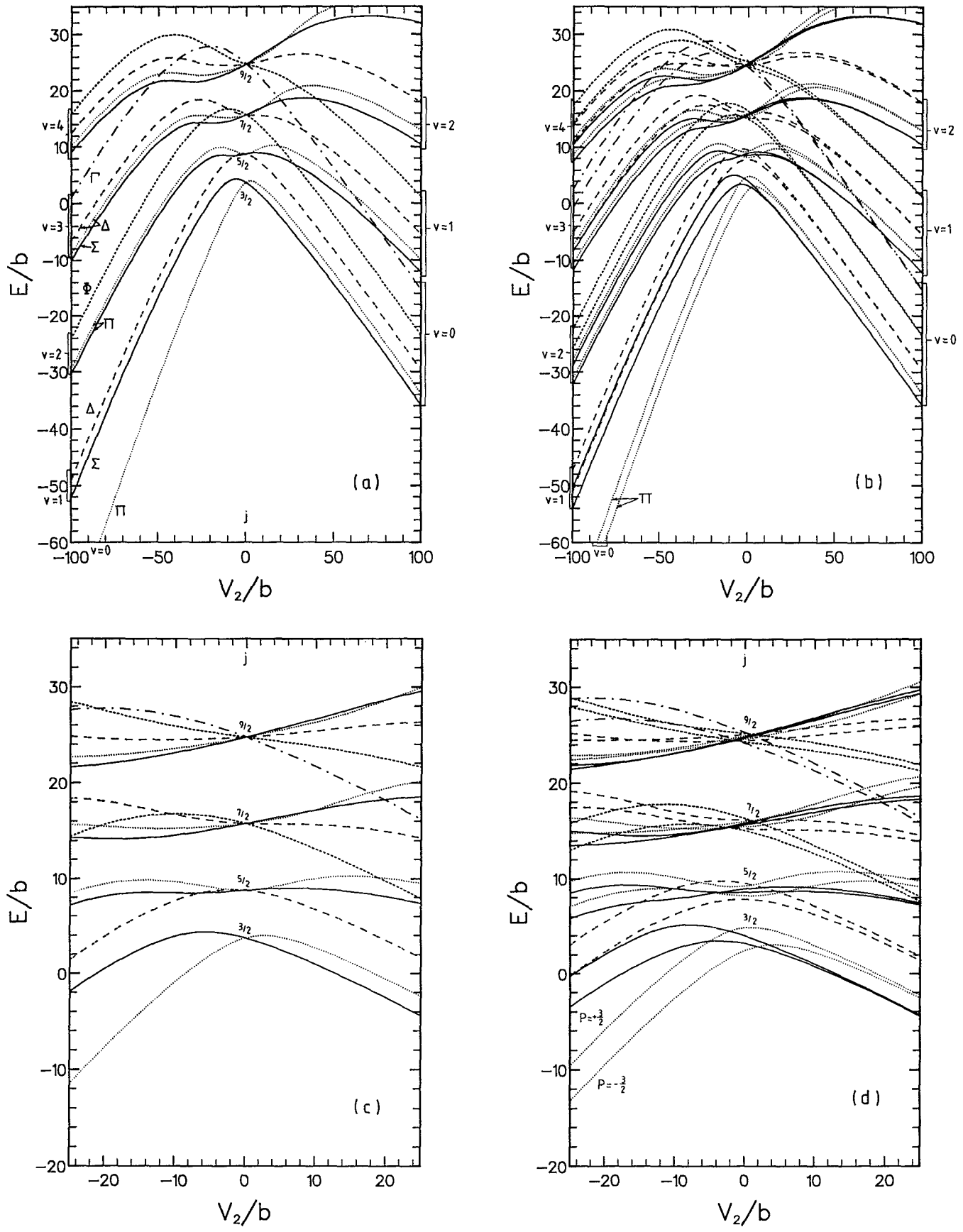

FIG. 5. Correlation diagrams for complexes containing diatoms in $^2\Pi_{3/2}$ states. Parts (a) and (b) show the bending energy levels as a function of the V_{20} anisotropy for $V_{10} = 0$ and $2b$, respectively. States with different values of the projection quantum number P are shown with different line types as indicated in Fig. 4(a). In the near-rigid linear limit, the states are given vibronic labels indicating the value of K. Parts (c) and (d) show expanded versions of the central regions of parts (a) and (b), respectively. All energies are shown in terms of the monomer rotational constant b.

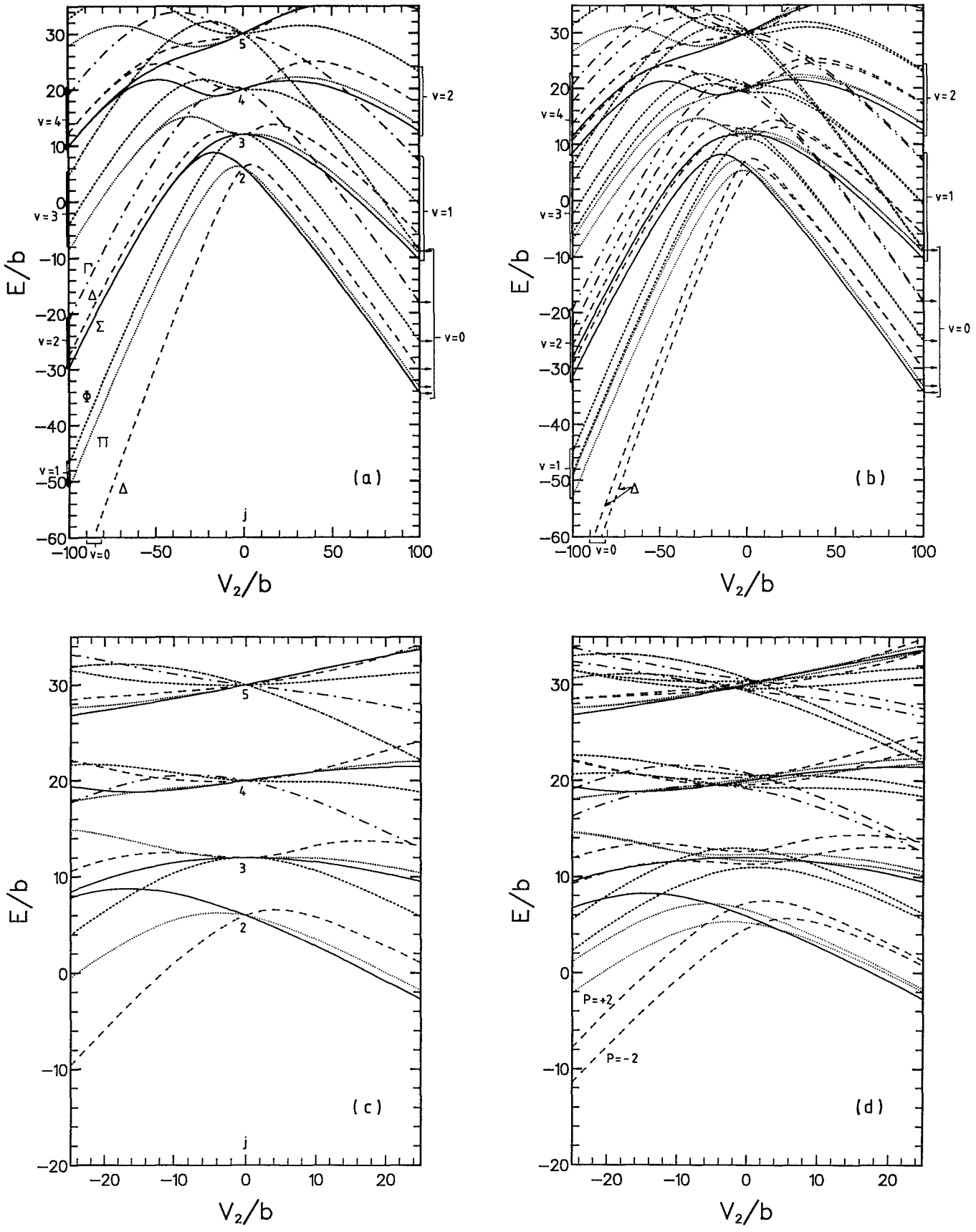

FIG. 6. Correlation diagrams for complexes containing diatoms in $^3\Pi_2$ states. Parts (a) and (b) show the bending energy levels as a function of the V_{20} anisotropy for $V_{10} = 0$ and $2b$, respectively. States with different values of the projection quantum number P are shown with different line types as indicated in Fig. 2(a). In the near-rigid linear limit, the states are given vibronic labels indicating the value of K. Parts (c) and (d) show expanded versions of the central regions of parts (a) and (b), respectively. All energies are shown in terms of the monomer rotational constant b.

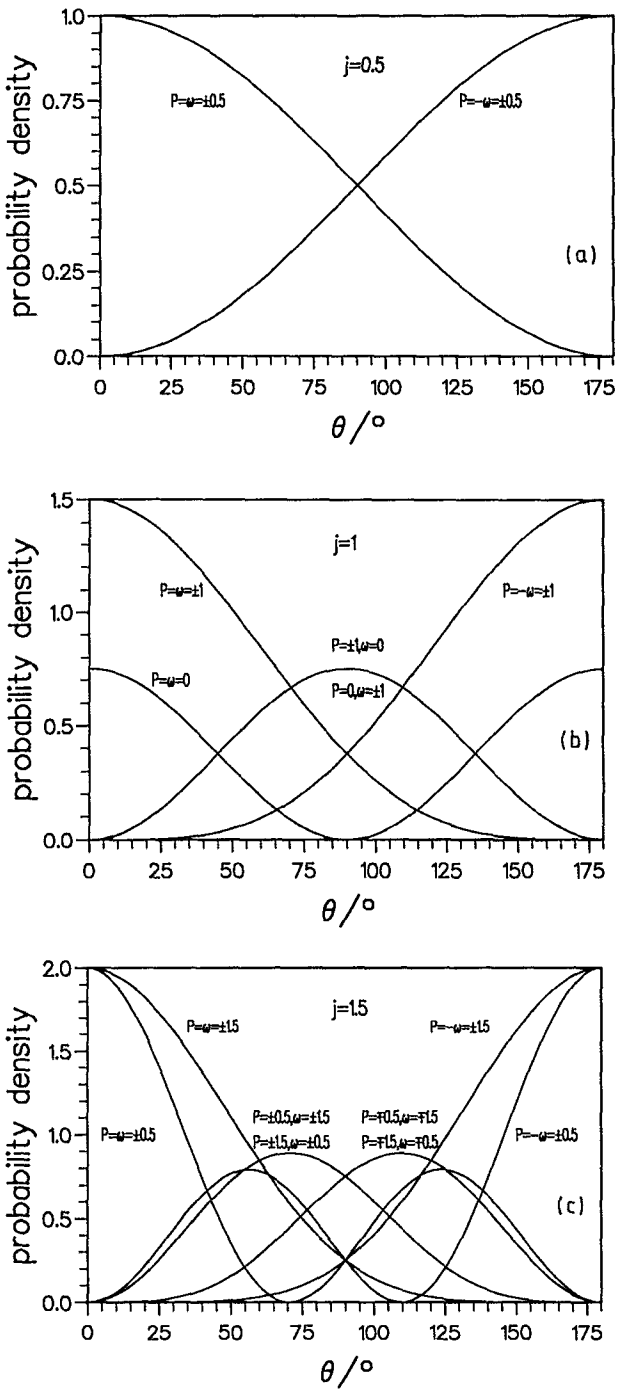

FIG. 7. Free-rotor angular probability density functions $(j+\frac{1}{2})[d^{j}_{P\omega}(\theta)]^2$ for diatoms in Hund's case (a).

Complexes such as Ar–OH and Ne–OH in their ground electronic states lie quite close to the center of the diagrams in Fig. 5. Their energy levels are characterized by quantum numbers j, ω, J, and P. The relative sign of ω and P is significant, but the two quantum numbers refer to projections along different axes, so that it is *not* appropriate to define a vibronic quantum number Λ (or K).

The large-anisotropy limits of the correlation diagrams for diatoms in Π states may be understood by generalizing the arguments used for Σ states. For large negative V_{20} the energy levels are again those of a linear triatomic molecule: the vibrational angular momentum l runs from $-v_2$ to $+v_2$ in steps of 2. In this limit (but *only* in this limit), $\omega=\lambda+\sigma$ lies along the intermolecular axis, so that it is justified to couple the free monomer quantum number ω with the vibrational angular momentum and to write $P=l+\omega$. The states are described by P and the associated spin–free quantum number $K=l+\lambda$, and may be characterized by vibronic labels such as $^2\Pi_{3/2}$ (indicating $K=1$, $P=\frac{3}{2}$). However, it must be emphasized that such labels are a poor description of the free-rotor limit, and should *not* be used except in complexes with very high anisotropy.

We now consider the correlation diagrams in Figs. 3–6 in more detail. The correlation diagrams for $^1\Pi_1$ state diatoms are shown in Fig. 3, again for $V_{10}=0$ and $V_{10}=2b$. As for Σ states, the V_{20} anisotropy splits each free-rotor state into $j+1$ components with different values of $|P|$. As expected (but by contrast with the Σ state case) the V_{10} anisotropy causes first-order splittings even for $V_{20}=0$: each diatom j state is split into $2j+1$ separate components with different values of P. The splittings due to V_{10} collapse with increasing positive V_{20}, so that the T-shaped limits are similar in Fig. 3(a) and 3(b). In the linear limit, the lowest level in Fig. 3 ($v_2=0$, $l\equiv R=0$) has $P=K=1$, and may be described as a $^1\Pi_1$ vibronic state. The first excited bending level ($v_2=1$, $l=1$) is split by coupling with λ into components with $P\equiv K=0$ and 2 ($^1\Sigma_0$ and $^1\Delta_2$ vibronic states). The second excited level ($v_2=2$, $l=0$ and 2) is split into 2 components with $P=1$ and 3. Note that the $l=0$ and $l=2$ components of the $P=1$ state are degenerate in this approximation. However, this degeneracy is resolved when higher-order spherical harmonic terms (e.g., V_{22}, V_{40}) are included in the potential expansion. This is a general feature: unexpected degeneracies of levels with the same P but different l and ω sometimes appear in the near-rigid linear limit for simple potentials, but are removed for more realistic potentials.

As mentioned above, the levels of closed-shell complexes for large negative V_{20} exist as near-degenerate pairs that become nondegenerate because of tunnelling splittings as the barrier is decreased. However, for complexes of Π state diatoms the situation is somewhat different: the transformation $\theta\rightarrow\pi-\theta$ leaves the potential unchanged, but alters the relative directions of ω and P. The two states that are mixed by the transformation are thus nondegenerate, and no splitting is observed as the barrier is decreased (except for $P=0$, for which tunnelling splittings occur exactly as in the closed-shell case).

Next we can examine the effect of spin, and compare the correlation diagrams for $^1\Pi_1$ with those for $^2\Pi_\omega$ and $^3\Pi_2$ monomers (Figs. 4–6). In the $^2\Pi_\omega$ case the V_{20} anisotropy splits each free-rotor state into $j+\frac{1}{2}$ components with different values of $|P|$, while the V_{10} anisotropy lifts the degeneracy of states with $\pm P$. In the near-rigid linear limit, the rules governing the patterns are the same as before but the relevant quantum number is now $P=l+\omega$ rather than $K=l+\lambda$. In each case the ground state has $l=0$ and $P=\omega$, while the first excited bending state has $l=1$ and is split into components with $P=\omega\pm1$. As mentioned above,

the correlation diagrams for $^3\Pi_0$ monomers are the same as for Σ state monomers (Fig. 2) and those for $^3\Pi_1$ monomers are the same as for $^1\Pi_1$ monomers (Fig. 3).

For Π state monomers, as for Σ state monomers, all the levels are doubly degenerate in the homonuclear case ($V_{10}=0$) because the potential well has a symmetric double minimum structure. This degeneracy is resolved in the heteronuclear case ($V_{10}\neq 0$) because the wells at $\theta=0$ and $\theta=180°$ are different, so each well gives rise to a set of equally spaced bending levels; the two sets have origins differing by $2V_{10}$ and slightly different vibrational spacings. In the large-anisotropy limit, the effect of V_{10} is similar in the open-shell and closed-shell cases.

Despite the similarities of the correlation diagrams for large anisotropies, there are important differences for small anisotropies. Parts (c) and (d) of each of Figs. 3–6 show expanded versions of the central sections of parts (a) and (b). This is the relevant region for most Van der Waals complexes in their ground electronic states, and the energy levels are best described in terms of diatom free-rotor quantum numbers rather than bending vibrational quantum numbers.

An important difference between the diagrams for different ω values arises because the lowest allowed diatom rotational level has $j=\omega$. The energy spacing between this level and the next is thus $2b(\omega+1)$ in the free-rotor limit for Hund's case (a); this is $2b$ for a closed-shell diatom, $3b$ for a $^2\Pi_{1/2}$ diatom, and $5b$ for a $^2\Pi_{3/2}$ diatom. Since the mixing of rotational levels induced by the potential anisotropy is inversely proportional to this spacing, complexes containing monomers with large ω are closer to the free-rotor limit than similarly anisotropic complexes with lower values of ω. The ground state of OH is $^2\Pi_{3/2}$, with the result that the bending levels of both Ar–OH and Ne–OH are very close to the free-rotor limit: the free-rotor levels are split and shifted, but not greatly mixed, by the anisotropy.

It may be seen from Figs. 3 to 6 that the energy levels are quite well approximated by first-order expressions for $V_{20}<5b$ (or rather more for higher values of ω). Beyond that, the correlations are governed by the rule that different states of the same P cannot cross. States of different P are not coupled by the potential, so can cross in the approximation used here; however, it should be remembered that there are in fact Coriolis matrix elements of order BJj off-diagonal in P by ± 1; this will introduce P-type doubling in the spectrum, and more substantial perturbations may be expected when states with $\Delta P=\pm 1$ are near degenerate.

1. Angular momentum decoupling effects for $^2\Pi$ monomers

As mentioned above, deviations from pure case (a) coupling are quite important for monomers such as OH. The energy levels of pure case (a) monomers in $^2\Pi_{1/2}$ and $^2\Pi_{3/2}$ states are given by Eqs. (4) above. The only nonzero matrix element of $H_{\rm mon}$ between these two substates is given by the $(\hat{j}_-\hat{s}_+ + \hat{j}_+\hat{s}_-)$ part of the Hamiltonian (3),

$$\langle ^2\Pi_{3/2}\, j|H_{\rm rot}|^2\Pi_{1/2}\, j\rangle = -b\left[(j+\tfrac{1}{2})^2-1\right]^{1/2}. \qquad (37)$$

In complexes near the free-rotor limit, this interaction couples states with the same values of j and P but differing in ω by ± 1. It can cause quite substantial shifts of the monomer energy levels, even for low values of j: in OH $X\,^2\Pi_{3/2}$, for example, it shifts the $j=\frac{3}{2}$ state by $-5.7\ \mathrm{cm}^{-1}$ and the $j=\frac{5}{2}$ state by $-14.5\ \mathrm{cm}^{-1}$, and these shifts remain in the complex. However, the shifts do not (in first order) depend on P, so that the pattern of P levels for each j is not qualitatively altered. For large j values it would be advantageous to use a case (b) basis set for the diatomic molecule, but this is not necessary for the levels observed so far.

Transitions between states differing in ω by ± 1 are forbidden for pure case (a) coupling (though they become allowed when decoupling effects are included). The decoupling effects will thus not produce any relaxation of selection rules in the complex for transitions within a given ladder of ω states, though they will allow direct far-infrared transitions with $\Delta\omega=\pm 1$. For Ar–OH these lines are likely to be broadened by electronic predissociation of the OH $^2\Pi_{1/2}$ complex to form OH $^2\Pi_{3/2}$ products.

For near-rigid linear complexes, the effect of a large $b(\hat{j}_-\hat{s}_+ + \hat{j}_+\hat{s}_-)$ term is to mix states of different ω. Under these circumstances, the high-anisotropy states are not simply the union of those in Figs. 4 (for $^2\Pi_{1/2}$ monomers) and 5 (for $^2\Pi_{3/2}$ monomers). When the decoupling term is omitted, there are separate (nondegenerate) levels for each allowed combination of v, ω, and P. However, when the decoupling is large, some pairs of states of different P become near-degenerate. The resulting correlation diagram is shown in Fig. 8, and is best explained in terms of a spin–orbit splitting superimposed on the pattern for a $^1\Pi$ monomer (Fig. 3): every K level is split by spin–orbit coupling into levels with $P=K\pm s$, with a splitting almost equal to the monomer spin–orbit coupling constant. The degeneracies between different l states contributing to the same K are preserved in the presence of decoupling (but are resolved by V_{22}, see below).

2. λ doubling

λ doubling in Π state monomers arises from matrix elements of $H_{\rm mon}$ off-diagonal in λ: it is caused by the operators $(b+\frac{1}{2}a)(\hat{l}_+\hat{s}_- + \hat{l}_-\hat{s}_+)$ and $b(\hat{j}_+\hat{l}_- + \hat{j}_-\hat{l}_+)$ from Eq. (3). In the effective Hamiltonian for the monomer in the signed ω basis, there are matrix elements with $\Delta\lambda=\pm 1$ and $\Delta\sigma=0$ or ∓ 1.[46] For the OH monomer the $j=\frac{1}{2}$, $\omega=\frac{1}{2}$ level is split into two components separated by $0.260\ \mathrm{cm}^{-1}$, while the $j=\frac{3}{2}$, $\omega=\frac{3}{2}$ level is split into two components separated by $0.055\ \mathrm{cm}^{-1}$.

For complexes near the free-rotor limit, λ doubling occurs only in the absence of a V_{10} anisotropy (i.e., for complexes of homonuclear diatoms). For complexes of heteronuclear diatoms, the V_{10} anisotropy separates the components with positive and negative values of ω as discussed above: under these circumstances the λ-doubling matrix elements merely cause a small additional shift of the components, without introducing an extra splitting. Provided there is a V_{10} anisotropy, this behavior persists in the linear near-rigid limit, and there is no significant λ doubling.

Even in the absence of a V_{10} anisotropy, the λ doubling is very quickly quenched by a negative V_{20} anisotropy. We

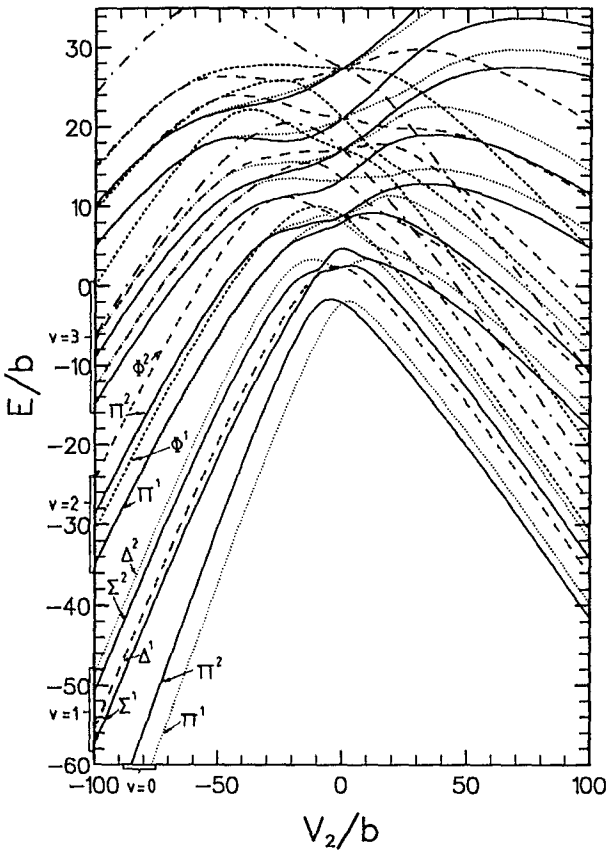

FIG. 8. Correlation diagram for complexes containing diatoms in $^2\Pi$ states, including terms coupling $^2\Pi_{1/2}$ and $^2\Pi_{3/2}$ manifolds, for $V_{10} = 0$. The value of the spin–orbit coupling constant used here, $a = -7.503b$, is appropriate for OH $X\,^2\Pi$. States with different values of the projection quantum number P are shown with different line types as indicated in Fig. 4(a) The vibronic labels Σ, Π, Δ, etc. on the left-hand side indicate the value of K, and the superscripts 1 and 2 indicate levels arising principally from $\omega = \frac{1}{2}$ and $\frac{1}{2}$, respectively. All energies are shown in terms of the monomer rotational constant b.

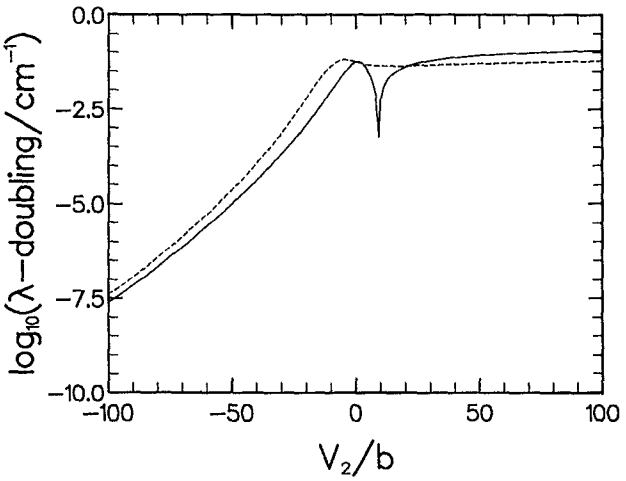

FIG. 9. The magnitude of the λ-doubling splitting as a function of anisotropy for λ-doubling parameters appropriate to OH $X\,^2\Pi$. The solid line is for the lowest $|\omega| = \frac{1}{2}$ state, and the dashed line for the lowest $|\omega| = \frac{3}{2}$ state. Note the logarithmic energy scale: the cusp in the solid curve indicates a crossing between the λ-doubling components for $|\omega| = \frac{3}{2}$.

constructed the effective λ doubling Hamiltonian in the free-rotor basis set, and then transformed it into the basis set formed by the eigenvectors of the remainder of the Hamiltonian. Unfortunately the splittings are too small to show usefully on correlation diagrams, but for λ-doubling parameters the size of those in OH there are two types of matrix element of significance: a very small matrix element connecting the two states with $P = \frac{3}{2}$, $\omega = \pm\frac{3}{2}$, and a much larger matrix element (0.3 to 0.5 cm^{-1}) connecting each of these states to (different) excited bending states. However, the latter matrix elements have exactly the same effect for the two components of the λ doublet. The splitting is entirely due to the direct coupling matrix element, which decreases almost exponentially with V_{20}; the resulting splitting is shown in Fig. 9. In the linear near-rigid limit, therefore, the λ doubling is very much smaller than in the monomer.

The behavior for positive V_{20} anisotropies is somewhat different: the λ doubling in these circumstances is only slightly different from that for the free monomer (see Fig. 9). However, for T-shaped complexes involving heteronuclear diatoms there is a small matrix element of V_{10} anisotropy between the λ-doubling levels, so that the states are again best described by signed ω quantum numbers.

It should be emphasized that the discussion above refers entirely to the role of the *monomer* λ doubling in the complex, and deals with splittings that depend on the monomer rotational quantum number j. It does *not* refer to P-type doubling in the complex as a whole, which produces splittings dependent on the total angular momentum J.

3. The Renner-Teller effect

It is well known that Π electronic states of triatomic linear molecules exhibit the Renner–Teller effect, because of the existence of two nondegenerate potential energy surfaces for nonlinear geometries. In Van der Waals complexes containing monomers in Π states, the Renner–Teller effect is provided by the V_{22} anisotropy. This section will investigate the effect of a V_{22} anisotropy on the energy levels, concentrating on the "linear molecule" limit with a large negative value of V_{20}.

The V_{22} anisotropy mixes and shifts levels with $\Delta\lambda = \pm 2$. For a $^1\Pi$ monomer, for given values of v and K with $K < v + 1$, V_{22} splits the pairs of levels with $\omega = \lambda = +1$ and $\omega = \lambda = -1$. The only levels that are not split are those with $K = v + 1$, since there is only one way to couple $\omega = \lambda$ and l to get $K = v + 1$. These are the "unique levels" described by Jungen and Merer.[47]

For a $^2\Pi$ monomer, the situation is a little more complicated. For a given P and v, V_{22} again mixes and shifts pairs of levels with $\Delta\lambda = \pm 2$. However, since V_{22} is diagonal in σ, the two levels in this case must belong to different spin–orbit manifolds, with $\omega = \pm\frac{3}{2}$ and $\omega = \mp\frac{1}{2}$. For low bending vibrational levels ($v = 0,1$), V_{22} causes only slight shifts. For $v > 1$, there are some values of P that occur in both spin–orbit manifolds, and V_{22} mixes these. The effect is shown in Fig. 10 for $v = 3$: in the absence of V_{22} there are two doublets, each containing $|P| = \frac{1}{2}$ and $\frac{3}{2}$ states. In the presence of V_{22} the degeneracy is lifted and the upper doublet is inverted be-

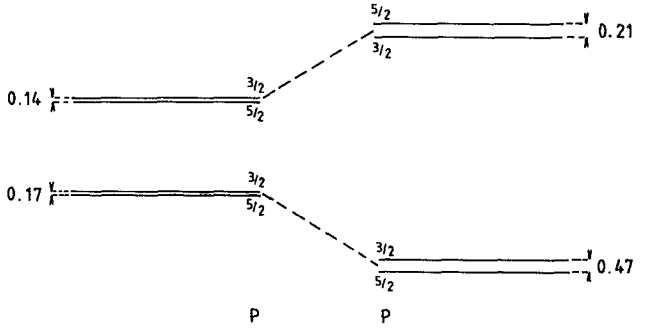

FIG. 10. The effect of a V_{22} anisotropy on $v = 3$ bending energy levels for the case of a near-rigid linear complex in a $^2\Pi$ electronic state.

cause the $P = \frac{3}{2}$ states are pushed apart by less than the $P = \frac{5}{2}$ states.

V. APPLICATION TO Ar–OH AND Ne–OH

Electronic spectra of Ar–OH, correlating with the $A \leftarrow X$ band system of OH, have been observed by Lester and co-workers[15–19] and Fawzy and Heaven.[20,21] Similar spectra of Ne–OH have been observed by Lin *et al.*[26] Attempts to measure microwave and infrared spectra of these complexes are in progress. This section will discuss the nature of the spectra obtained so far, including the selection rules applicable and the structures that are to be expected at higher resolution. It will also discuss the nature of the infrared and far-infrared spectra to be expected for Ar–OH and Ne–OH.

A. Energy level patterns and quantum numbers

Degli Esposti *et al.*[24] have carried out high-level *ab initio* calculations on the potential energy surfaces for Ar interacting with OH in its $X\,^2\Pi$ and $A\,^2\Sigma$ states. They obtained a ground state surface with a spherically averaged well depth of about 69 cm^{-1} at $R \approx 3.72$ Å. The anisotropic coefficients at this distance are $V_{10} = -15.7$ cm^{-1}, $V_{20} = -15.4$ cm^{-1} and $V_{22} = 22.4$ cm^{-1}. By contrast, the excited state surface is strongly bound and very anisotropic, with deep wells about 1000 cm^{-1} deep at the two linear geometries but a Van der Waals well only about 67 cm^{-1} deep at the T-shaped geometry. These potentials will be referred to below as the DEW potentials.

In the ground electronic state of OH, $b = 18.53$ cm^{-1} and the separation between the lowest two rotational states, $j = \frac{3}{2}$ and $\frac{5}{2}$, is 84 cm^{-1}.[48] The potential anisotropy is thus not strong enough to cause substantial mixing of the free-rotor states, and the levels are well described by free-rotor quantum numbers. The anisotropy *is* strong enough to quantize j along the intermolecular axis, with projection P. The quantum numbers describing the rotational levels of Ar–OH ($X\,^2\Pi$) are thus j, ω, J, P, and the total parity; the splittings for the lowest few j levels are shown in Fig. 11. The ground state has $P = \omega = \pm\frac{3}{2}$, and is thus in some respects analogous to a $^2\Pi_{3/2}$ vibronic state, but such labels are not appropriate to the states in general.

B. Selection rules and spectra

The space-fixed components of the transition dipole of a complex such as Ar–OH may be expanded in terms of body-fixed basis functions,

$$\mu_M = \sum_{jK} \mu_{jK}^{BF}(R)(4\pi)^{-1}[3(2j+1)]^{1/2} \times \mathscr{D}^{1*}_{MK}(\alpha,\beta,0)\mathscr{D}^{j*}_{K,\Delta\lambda}(\phi,\theta,0), \tag{38}$$

where $\Delta\lambda = \lambda_i - \lambda_f$. If electronic rearrangement is neglected, the transition dipoles responsible for spectroscopic transitions in Ar–OH and Ne–OH arise principally from dipoles fixed in the OH monomer. The space-fixed Z components of such dipoles may be written

$$\mu_Z = \mu_{OH} \sum_K \mathscr{D}^{1*}_{0K}(\alpha,\beta,0)\mathscr{D}^{1*}_{K,\Delta\lambda}(\phi,\theta,0). \tag{39}$$

The matrix elements of these operators between basis functions of the type (29) involve integrals of the form

$$\langle j_i P_i \omega_i | \mathscr{D}^{j*}_{K,\Delta\lambda} | j_f P_f \omega_f \rangle = (4\pi)^{-1}[(2j_i+1)(2j_f+1)]^{1/2} \int \mathscr{D}^{j_i}_{P,\omega_i}(\phi,\theta,0)\mathscr{D}^{j*}_{K,\Delta\lambda}(\phi,\theta,0)\mathscr{D}^{j_f*}_{P_f\omega_f}(\phi,\theta,0)\,d\phi \sin\theta\, d\theta\, \delta_{\sigma,\sigma_f}$$

$$= (-1)^{P_i-\omega_i}[(2j_i+1)(2j_f+1)]^{1/2} \begin{pmatrix} j_i & j & j_f \\ -\omega_i & \Delta\lambda & \omega_f \end{pmatrix} \begin{pmatrix} j_i & j & j_f \\ -P_i & K & P_f \end{pmatrix}. \tag{40}$$

1. Far-infrared spectra

The dipole moment responsible for far-infrared transitions in Ar–OH arises principally from the dipole moment of the OH monomer itself, and lies along the OH axis. Its space-fixed Z component is therefore as in Eq. (39) with $\Delta\lambda = 0$. The resulting selection rules from Eq. (40) are thus $\Delta j = 0, \pm 1$ and $\Delta P = 0, \pm 1$. For Ar–OH, the only strongly allowed transitions out of the ground state will be to the $j = \frac{3}{2}, \omega = \pm\frac{3}{2}, P = \pm\frac{1}{2}$ state (band origin around 13 cm^{-1} for the DEW potential) and the $j = \frac{5}{2}$, $\omega = \pm\frac{3}{2}$, $P = \pm\frac{5}{2}, \pm\frac{3}{2}, \pm\frac{1}{2}$ states (band origins between 90 and 95 cm^{-1}). The transition to the $j = \frac{3}{2}, \omega = \pm\frac{3}{2}, P = \mp\frac{1}{2}$ state (around 20 cm^{-1}) is forbidden except for the mixing of states with $\Delta P = \pm 1$ by the $\hat{\mathbf{j}}\cdot\hat{\mathbf{J}}$ term in the Hamiltonian: it will be weaker than the $P = \pm\frac{3}{2} \rightarrow \pm\frac{1}{2}$ transition by a factor of about $(BJj/\Delta E)^2$, where ΔE is the spacing between the $P = \mp\frac{1}{2}$ and $\pm\frac{1}{2}$ states, which is about 7 cm^{-1} for Ar–OH. This latter prediction is in agreement with the corrected simulations of the infrared spectrum of Ar–OH by Chakravarty and Clary.[23] The $j = \frac{5}{2}$ states are above the threshold for rotational predissociation on the DEW potential, but might be

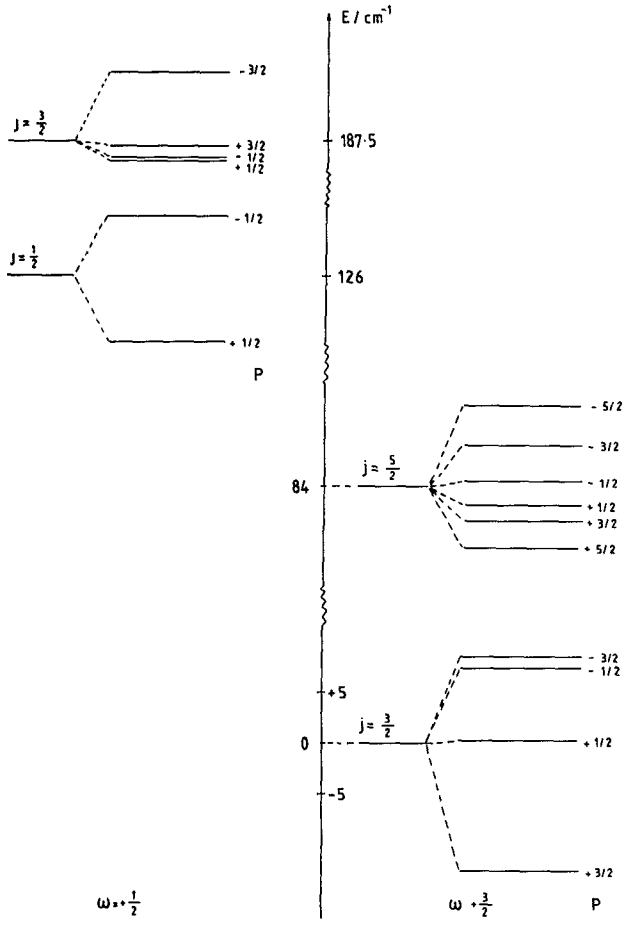

FIG. 11. Bending energy levels and assignments for Ar–OH in the $X\,^2\Pi$ state, showing the correlation with the OH free-rotor levels.

bound if the true well depth is 25 cm^{-1} or more deeper than the theoretical one. The analogous states may be expected to be bound for heavier rare gases or more strongly bound molecular perturbers.

2. Near-infrared spectra

Ar–OH and Ne–OH will also have spectra correlating with vibrational excitation of the OH monomer. The evidence from the spectroscopy of complexes such as Ar–HCl (Refs. 49–52) is that intermolecular potentials change only slightly on monomer vibrational excitation, so that the ladder of intermolecular vibrations built upon OH ($v=1$) may be expected to be very similar to that built upon OH ($v=0$) (though there is in fact a quite substantial change in the monomer rotational constants between $v=0$ and 1.)[48] The infrared spectrum appearing in the OH stretching region will thus be similar in structure to the far-infrared spectrum, except for the effects of vibrational predissociation.

3. Electronic spectra

The transition dipole responsible for the $A \leftarrow X$ electronic transition in OH is perpendicular to the OH axis. This provides a major contribution to the corresponding transition dipole in the complexes, with a space-fixed Z component given by Eq. (39) with $\Delta\lambda = \pm 1$. However, higher j values from Eq. (38) may also be important, especially for Ar–OH.

In calculating matrix elements between the basis functions for Π state monomers, Eq. (29), and those of case (A) or case (B) functions for Σ state monomers, Eqs. (16) or (21), it is necessary to include a rotation matrix to account for the different quantisation axes of the electron spin in the three cases. This is simplest for case (A), where we may write

$$\psi_{s\Sigma} = \sum_{\sigma} \mathscr{D}^{s*}_{\Sigma\sigma}(\phi,\theta,0)\psi_{s\sigma}. \tag{41}$$

Then, since[45]

$$\begin{aligned} &Y_{r\mathscr{R}}(\theta,\phi)\mathscr{D}^{s*}_{\Sigma\sigma}(\phi,\theta,0) \\ &\quad = (-1)^{P-\sigma}\sum_{j}(2j+1)\left(\frac{2r+1}{4\pi}\right)^{1/2}\begin{pmatrix} r & s & j \\ \mathscr{R} & \Sigma & -P \end{pmatrix} \\ &\qquad \times\begin{pmatrix} r & s & j \\ 0 & \sigma & -\sigma \end{pmatrix}\mathscr{D}^{j*}_{P\sigma}(\phi,\theta,0), \end{aligned} \tag{42}$$

the transition dipole integrals required may then be expressed in terms of the integrals of Eq. (40),

$$\begin{aligned} &\int \sum_{\sigma_i} Y^*_{r_i\mathscr{R}_i}(\theta,\phi)\mathscr{D}^{s}_{\Sigma,\sigma_i}(\phi,\theta,0)\mathscr{D}^{j*}_{K,\pm 1}(\phi,\theta,0) \\ &\qquad \times\left(\frac{2j_f+1}{4\pi}\right)^{1/2}\mathscr{D}^{j_f*}_{P_f\omega_f}(\phi,\theta,0)\,d\phi\,\sin\theta\,d\theta\,\delta_{\sigma,\sigma_f} \\ &\quad = \sum_{j_i}\left[(2r+1)(2j_i+1)\right]^{1/2}\begin{pmatrix} r_i & s & j_i \\ \mathscr{R}_i & \Sigma_i & -P_i \end{pmatrix} \\ &\qquad \times\begin{pmatrix} r_i & s & j_i \\ 0 & \sigma_f & -\sigma_f \end{pmatrix}\langle j_iP_i\sigma_f|\mathscr{D}^{j*}_{K,\pm 1}|j_fP_f\omega_f\rangle. \end{aligned} \tag{43}$$

If the transition dipole term with $j=1$ is dominant, the resulting selection rules are $j_f = r_i \pm \frac{1}{2}$ or $r_i \pm \frac{3}{2}$ and $\Delta P = \pm 1$.

For Ar–OH, the levels correlating with the $A\,^2\Sigma$ state of OH experience a strongly anisotropic potential with a deep primary minimum at the linear Ar–H–O geometry, $\theta = 0$, and a slightly shallower secondary minimum at the linear Ar–O–H geometry. The secondary minimum is deep enough to support bound states. However, as shown in Fig. 7, the ground bending state of Ar–OH ($X\,^2\Pi$), with $j=\frac{1}{2}$ and $P=\omega=\pm\frac{1}{2}$, samples mainly geometries around $\theta=0$, so that the Franck–Condon factors favor transitions to excited states in the primary well. Conversely, if levels such as the $j=\frac{3}{2}, \omega=-P=\pm\frac{1}{2}$ state could be populated, the Franck–Condon factors would then favor transitions to excited states in the secondary well.

Ne–OH is a rather different case, with a much weaker anisotropy in the excited state. Lin *et al.*[26] have observed four bands of Ne–OH, designated α, β, γ, and δ, and three bands of Ne–OD, designated ϵ, ζ, and η. All these involve the ground vibrational state of the X manifold. The excited states of the α and ϵ bands have rotational constants around 0.18 cm^{-1}, and are probably due to excitation of states with no quanta in the intermolecular stretch, while the other bands have much smaller rotational constants, around 0.15 cm^{-1}, and are probably due to excitation of states with one

quantum in the intermolecular stretch. It appears that the electronically excited Ne–OH states are best described by free-rotor quantum numbers rather than bending vibrational quantum numbers: the most likely assignment for the excited states is that the β and ζ bands involve the $r=0$, $\mathscr{R}=0$ levels, while the δ and η bands involve the $r=1$, $\mathscr{R}=1$ (Π bend) levels. The γ band would then involve the $r=1$, $\mathscr{R}=0$ (Σ bend) level. As for Ar–HCl[49–52] and Ar–HF,[53] the Σ bend lies below the Π bend even though it correlates with the overtone of the Π bend in the near-rigid limit. In a first-order treatment, the Π bend lies $-\frac{3}{5}V_{20}$ above the Σ bend: this splitting is 13 cm^{-1} for Ne–OH,[26] allowing the value of V_{20} averaged over the intermolecular stretching motion to be estimated as about -22 cm^{-1}. The separation between the ground state and the Π bend, which should be $2b-\frac{1}{5}V_{20}$ in the first-order model, is predicted (observed) on this basis to be 38.3 cm^{-1} (32.5 cm^{-1}) and 22.4 cm^{-1} (22.8 cm^{-1}) for Ne–OH and Ne–OD, respectively: this provides qualitative support for the assignment, while illustrating the effects of neglecting higher-order terms and bend-stretch coupling.

VI. CONCLUSIONS

We have investigated the energy level patterns for Van der Waals complexes containing open-shell monomers, as a function of the strengths of potential anisotropies of various kinds. For monomers in multiplet Σ states, coupling cases analogous to Hund's coupling cases have been identified: the coupling case that actually occurs for any given Van der Waals complex depends on the relative magnitudes of the monomer spin–rotation coupling constant, the potential anisotropy and the rotational constant of the complex. For monomers in Π states, the energy levels are analogous to those of atom-symmetric top complexes. In particular, a V_{10} anisotropy can affect the energy levels in first order; this does not happen for $^1\Sigma$ diatoms. The effect of V_{10} depends on the *sign* of the monomer projection quantum number ω relative to the body-fixed projection number P for the complex: it is thus appropriate to describe the energy levels of the complex in a signed-ω basis rather than in the symmetrised basis set usually used for the free monomer.

ACKNOWLEDGMENT

This work is supported by the Science and Engineering Research Council.

[1] J. M. Hutson, Annu. Rev. Phys. Chem. **41**, 123 (1990).
[2] R. J. Le Roy and J. van Kranendonk, J. Chem. Phys. **61**, 4750 (1974).
[3] R. J. Le Roy and J. S. Carley, Adv. Chem. Phys. **42**, 353 (1980).
[4] R. J. Le Roy and J. M. Hutson, J. Chem. Phys. **86**, 837 (1987).
[5] S. L. Holmgren, M. Waldman, and W. Klemperer, J. Chem. Phys. **69**, 1661 (1978).
[6] J. M. Hutson and B. J. Howard, Mol. Phys. **43**, 493 (1981).
[7] J. M. Hutson and B. J. Howard, Mol. Phys. **45**, 769 (1982).
[8] J. M. Hutson and B. J. Howard, Mol. Phys. **45**, 791 (1982).
[9] J. M. Hutson, J. Chem. Phys. **89**, 4550 (1988).
[10] J. M. Hutson, J. Chem. Phys. **91**, 4448 (1989).
[11] J. M. Hutson, J. Chem. Phys. **91**, 4455 (1989).
[12] D. J. Nesbitt, M. S. Child, and D. C. Clary, J. Chem. Phys. **90**, 4855 (1989).
[13] J. M. Hutson, J. Chem. Phys. **92**, 157 (1990).
[14] R. C. Cohen and R. J. Saykally, J. Phys. Chem. **94**, 7991 (1990).
[15] M. T. Berry, M. R. Brustein, J. R. Adamo, and M. I. Lester, J. Phys. Chem. **92**, 5551 (1988).
[16] M. T. Berry, M. R. Brustein, and M. I. Lester, Chem. Phys. Lett. **153**, 17 (1988).
[17] M. T. Berry, M. R. Brustein, and M. I. Lester, J. Chem. Phys. **90**, 5878 (1989).
[18] K. M. Beck, M. T. Berry, M. R. Brustein, and M. I. Lester, Chem. Phys. Lett. **162**, 203 (1989).
[19] M. T. Berry, M. R. Brustein, and M. I. Lester, J. Chem. Phys. **92**, 6469 (1990).
[20] W. M. Fawzy and M. C. Heaven, J. Chem. Phys. **89**, 7030 (1988).
[21] W. M. Fawzy and M. C. Heaven, J. Chem. Phys. **92**, 909 (1990).
[22] C. Chakravarty, D. C. Clary, A. Degli Esposti, and H.-J. Werner, J. Chem. Phys. **93**, 3367 (1990).
[23] C. Chakravarty and D. C. Clary, J. Chem. Phys. **91**, 4149 (1991).
[24] A. Degli Esposti and H.-J. Werner, J. Chem. Phys. **93**, 3351 (1990).
[25] J. M. Bowman, B. Gadzy, P. Schafer, and M. C. Heaven, J. Phys. Chem. **94**, 2226 (1990).
[26] Y. Lin, S. K. Kulkarni, and M. C. Heaven, J. Phys. Chem. **94**, 1720 (1990).
[27] Y. Lin, S. K. Kulkarni, and M. C. Heaven (to be published).
[28] Y. Lin, S. K. Kulkarni, and M. C. Heaven, Ohio State Spectroscopy Symposium, Columbus, Ohio, 1990.
[29] P. D. A. Mills, C. M. Western, and B. J. Howard, J. Phys. Chem. **90**, 3331 (1986).
[30] W. M. Fawzy and J. T. Hougen, J. Mol. Spectrosc. **137**, 154 (1989).
[31] P. D. A. Mills, C. M. Western, and B. J. Howard, J. Phys. Chem. **90**, 4961 (1986).
[32] P. D. A. Mills, D. Phil. thesis, Oxford University, 1982.
[33] H. Klar, J. Phys. B **6**, 2139 (1973).
[34] S. Green and R. N. Zare, Chem. Phys. **7**, 62 (1975).
[35] M. H. Alexander, J. Chem. Phys. **76**, 3637 (1982).
[36] M. H. Alexander, J. Chem. Phys. **76**, 5974 (1982).
[37] D. P. Dewangan and D. R. Flower, J. Phys. B **16**, 2157 (1983).
[38] G. C. Corey and F. R. McCourt, J. Phys. Chem. **87**, 2723 (1983).
[39] M. H. Alexander, Chem. Phys. **92**, 337 (1985).
[40] M. H. Alexander and G. C. Corey, J. Chem. Phys. **84**, 100 (1986).
[41] D. P. Dewangan, D. R. Flower, and M. H. Alexander, Mon. Not. R. Astron. Soc. **226**, 505 (1987).
[42] S. Bratoz and M. L. Martin, J. Chem. Phys. **42**, 1051 (1965).
[43] J. M. Hutson, Advances in Molecular Vibrations and Collision Dynamics **1**, 1 (1991).
[44] A. van der Avoird, J. Chem. Phys. **79**, 1170 (1983).
[45] D. M. Brink and G. R. Satchler, *Angular Momentum*, 2nd ed., (Clarendon Press, Oxford, 1968).
[46] J. M. Brown, M. Kaise, C. M. L. Kerr, and D. J. Milton, Mol. Phys. **36**, 553 (1978).
[47] Ch. Jungen and A. J. Merer, Mol. Phys. **40**, 1 (1980).
[48] J. A. Coxon, Can. J. Phys. **58**, 933 (1980).
[49] D. Ray, R. L. Robinson, D.-H, Gwo, and R. J. Saykally, J. Chem. Phys. **84**, 1171 (1986).
[50] R. L. Robinson, D.-H. Gwo, and R. J. Saykally, Mol. Phys. **63**, 1021 (1988).
[51] K. L. Busarow, G. A. Blake, K. B. Laughlin, R. C. Cohen, Y. T. Lee, and R. J. Saykally, Chem. Phys. Lett. **141**, 289 (1987).
[52] C. M. Lovejoy and D. J. Nesbitt, Chem. Phys. Lett. **146**, 582 (1988).
[53] C. M. Lovejoy and D. J. Nesbitt, J. Chem. Phys. **91**, 2790 (1989).